DESIGN AND EXPERIMENT OF DRAG REDUCTION CHARACTERISTICS OF CASSAVA BIONIC DIGGING SHOVEL BASED ON RED SOIL
/
基于红土壤的木薯仿生挖掘铲减阻特性设计与试验

Ranbing YANG[1,3], Guiquan ZHOU[1,3], Dongquan CHEN[2], Tao WANG[1,3], Danyang LV[2], Xiantao ZHA*[1,3]
[1] School of Mechanical and Electrical Engineering, Hainan University, Hainan/ China;
[2] School of Information and Communication Engineering, Hainan University, Hainan/ China;
[3] Key Laboratory of Tropical Intelligent Agricultural Equipment, Ministry of Agriculture and Rural Affairs, Hainan/ China;
Corresponding author: Xiantao Zha
Tel: +8618627838628; E-mail: zhaxt@hainanu.edu.cn
DOI: https://doi.org/10.35633/inmateh-74-56

Keywords: *Agricultural machinery, Cassava harvester, Digging shovel, Bionic, Drag reduction, Discrete element*

ABSTRACT
Aiming at the digging shovel of the red soil harvester in the cassava planting area, problems such as high digging resistance and difficulty in breaking the soil when harvesting cassava tubers will lead to blockage at the connection between the digging device and the transmission device. Using the rabbit's front paws as a bionic prototype, three-dimensional scanning and reverse engineering technologies were employed to extract their unique geometric features. These quantified geometric structural characteristics were then applied to the design of an excavation shovel, aiming to reduce resistance during excavation operations. Based on the discrete element (EDEM) coupled RECURDYN, using the resistance of the excavation shovel and the Bonding key breakage rate as evaluation indicators, the discrete element orthogonal analysis of three factors including the shovel tooth length, shovel tooth width, and shovel edge inclination angle was carried out based on the simulation test results. Test was performed to determine the best parameter combination for drag reduction and crushing rate of the bionic shovel; the working resistance of the shovel was used as an evaluation index to verify the excavation performance of the bionic shovel through field tests. The optimal parameter combination of the bionic shovel based on the discrete element simulation test is the tooth length of 220 mm, the tooth width of 65.1 mm, and the blade inclination 60°. The excavation resistance of this combination is 1733.66 N and the maximum soil fragmentation rate is 92.9%. Through field tests, it can be found that when the excavation depth is 310 mm and the forward speed is 300 mm/s. The Type 1 bionic digging shovel exhibits a reduction in resistance of 6.84%, while the Type 2 bionic digging shovel demonstrates a more significant reduction of 9.21%, compared to the traditional digging shovel. Tests have shown that the bionic shovel type 2 has excellent soil excavation characteristics and can complete cassava excavation operations in tropical red soil areas. It can provide a design reference for reducing drag and saving energy for cassava harvesters.

摘要
针对木薯种植区域的红土壤收获机挖掘铲在进行收获木薯块茎时挖掘阻力大、土壤破碎困难等问题会导致挖掘装置与传输装置连接处出现堵塞情况，以兔子的前爪为仿生原型，采用三维扫描和逆向工程技术提取其独特的几何特征。然后将这些量化的几何结构特征应用于挖掘铲的设计，旨在减少挖掘作业期间的阻力。基于离散元（EDEM）耦合 RECURDYN，以挖掘铲所受阻力、Bonding 键破碎率为评价指标，基于仿真试验结果进行了铲齿长度、铲齿宽度、铲刃倾角等3 个因素的离散元正交试验,确定仿生铲的减阻的和破碎率最佳的参数组合；通过田间试验以挖掘铲所受工作阻力为评价指标验证仿生挖掘铲的挖掘性能。基于离散元仿真试验可得的仿生铲最佳参数组合为铲齿长度 220mm、铲齿宽度 65.1mm、铲刃倾角 60°，该组合的挖掘阻力为 1733.66N 和较大的土壤破碎率为92.9%。通过田间试验可得挖掘深度为310mm、前进速为300mm/s 时，试验表明仿生铲 2 型有优秀的土壤挖掘特性，能在热带红土壤地区完成木薯挖掘作业，能为木薯收获机减阻节能做出设计参考。

[1,3] *Ranbing Yang, Prof. Ph.D. Eng; Guiquan Zhou, M.S. Stud. Eng; Tao Wang, Assoc. Prof. M. Eng; Xiantao Zha, Ph.D. Eng.*

[2] *Dongquan Chen, Ph.D. Eng; Danyang Lv, Ph.D. Eng.*

INTRODUCTION

Hainan Province is located in a tropical rain forest climate area *(Li et al., 2014)*. Under the conditions of high temperature, high humidity and high concentration of biological organic matter, it is easy to form red soil with heavy clay soil. However, cassava, which is highly adaptable to the environment and can grow in relatively harsh environments, is one of the excellent tropical economic crops. Observation in the practice of cassava planting fields shows that heavy soil is the main cause of resistance when the shovel is working. Therefore, when operating cassava harvesters under red soil conditions in tropical areas of Hainan Province, excavation drag reduction is the key technology to achieve high-efficiency and low-energy consumption harvesting of cassava.

Biomimetic design is a methodology that leverages biological structures, functions, and mechanisms found in nature to address engineering challenges and enhance performance by emulating the remarkable characteristics of natural systems. The extensive application of biomimetic and reverse engineering technologies within the engineering domain has demonstrated that simulation technology can effectively mitigate the challenges associated with limited experience in the design of mechanical components. The rise of bionics has led to practical applications demonstrating that bionic soil contact components can significantly save energy and reduce drag *(Cui et al., 2019; Zhang et al., 2022)*. The potato digging shovel is a critical soil-contacting component of agricultural machinery. Energy efficiency, drag reduction, and wear performance are essential indicators for these parts. Numerous scholars and research teams, both domestically and internationally, have conducted studies and provided substantial data supporting the development of bionic digging shovels *(Zhao et al., 2021)*.

For instance, *Fan Yu et al.* explored the excavation mechanism and aimed to reduce excavation resistance by employing discrete element analysis to examine the soil fragmentation principles from a microscopic perspective during the excavation process. They applied bionic design principles to the structure of the potato soil contact device, drawing inspiration from the arch mouth of wild boars. Subsequently, they coupled these external characteristics with the potato digging shovel and conducted a mechanical analysis of the tool. The test results indicate that the application of bionic theory can effectively reduce digging resistance during potato harvesting *(Fan et al., 2020)*.

Duanmu Lingjian et al. (2020) addressed the issues of high digging resistance and limited adaptability of cassava digging shovels by selecting the forepaw toes of the yellow-haired rat as a bionic prototype to design a shovel-toothed bionic digging shovel. This design effectively reduces drag and allows for adjustments in the number of teeth according to the specific needs of the digging shovel. Zou Xiangxiang and colleagues developed a bionic digging shovel inspired by the shape of the front toe claws of the Oriental mole cricket to tackle the challenges of inserting the digging shovel into the soil and achieving a low soil breaking rate during cassava harvesting *(Zou et al., 2013)*. Their analysis concentrated on the static strength of the cassava digging shovel structure using finite element analysis. *Sun et al.* designed a bionic trencher to address high resistance and viscosity issues encountered with trenchers, drawing from the hydrophobic drag-reducing characteristics of shell texture. This design effectively reduces drag, minimizes adhesion, and facilitates detachment *(Sun et al., 2020)*.

Yu et al. (2022) focused on the large digging resistance and complex root systems associated with potato digging shovels, creating a bionic shovel based on the outer contour of mole toes. They conducted a static strength analysis and a discrete element structural analysis of the digging shovel, employing both finite element and discrete element methods, which effectively reduced the traction power required by the harvester and enhanced the fatigue strength of the digging shovel.

In summary, the structural design of agricultural machinery that incorporates bionics can effectively reduce digging resistance during operation and enhance the soil crushing performance of such machinery. The focus of bionic structural design lies in the combination of appropriate bionic objects. This paper addresses the technical challenges posed by high clay resistance and the presence of heavy soil clods that are difficult to break in the red soil of Hainan's cassava cultivation. Using an ordinary cassava digging shovel as a prototype, the structure is enhanced by integrating the drag reduction curve of a rabbit claw's outer contour, along with the addition of an arched structure to optimize soil-breaking performance. The Bionic Rabbit Paw Cassava Digging Shovel is designed with reference to conventional digging shovels, aiming to achieve energy savings and reduced drag during operations.

MATERIALS AND METHODS

Analysis on the mechanism of excavating shovel resistance

When the excavating shovel is in operation, it can be divided into two distinct phases: penetrating the soil and excavating it. Bekker's semi-empirical formula is employed to develop a mathematical model that describes the volume of soil excavated, as well as the shear and normal stresses experienced during the penetration phase *(Zhang et al., 2015)*. Additionally, Rankine's earth pressure theory is applied to establish a mathematical model that elucidates the relationship between elastic soil properties and excavation depth during the soil excavation process *(Zhao et al., 2017; Li et al., 2023)*.

Excavating shovel force analysis

When the cassava digging shovel is working, the cassava digging shovel encounters four primary types of resistance, as illustrated in Figure 1. These include the positive pressure F_p exerted by the soil on the digging shovel, the frictional resistance F_{f1} between the soil and the digging shovel, the penetration resistance F_{f2} that occurs as the front end of the digging shovel penetrates the soil, and the inertial force F_a exerted by the soil on the digging shovel.

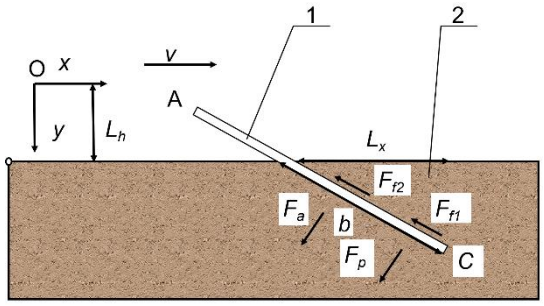

Fig. 1 - Force analysis of digging shovel during operation
1 – Digging shovel; 2 – Soil

Calculation of depth of penetration

As shown in Figure 1, O is the origin. The coordinates of points A and C and the distance L_h from the coordinate origin to the ground are known. It can be obtained that the horizontal projected length L_x of the digging shovel before it enters the soil and the length b of the digging shovel submerged in the soil are:

$$L_x = \frac{(y_c - L_h)(x_c - x_a)}{y_c - y_a} \quad (1)$$

$$b = \sqrt{L_x^2 + (y_c - L_h)^2} \quad (2)$$

where L_x is the horizontal length of the shovel into the soil; L_h is the distance from the coordinate origin to the ground; x_a is x coordinate of point A; y_a is y coordinate of point A; x_c is x coordinate of point C; y_c is y coordinate of point C; b is the length of the shovel into the soil.

Penetration resistance analysis and calculation

As shown in Figure 2, the angle of the shovel tip is θ, the excavating shovel width is d, and the shovel tip length is e. When the excavating shovel enters the soil, it is subject to the positive pressure F_σ of the soil on the excavating shovel and the shear stress F_τ of the soil on the excavating shovel. The penetration resistance when the front end of the digging shovel penetrates into the soil is F_{f2}.

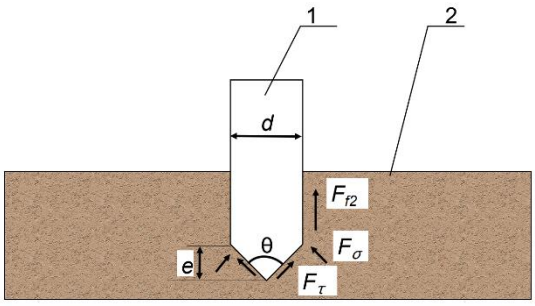

Fig. 2 - Stress analysis of shovel surface
1– Digging shovel; 2– Soil

It can be seen from Figure 2 that the geometric relationship between the blade tip length e, the angle θ between the excavation blade tip and the excavation blade width d is:

$$e = \frac{d}{2\tan(\theta/2)} \tag{3}$$

According to the relationship between digging shovel penetration and load in Bekker's semi-empirical formula, it can be obtained:

$$\sigma_y = \frac{k_1}{d} + k_2 y^n \tag{4}$$

$$\tau_{\max} = c_0 + \sigma_y \tan\alpha \tag{5}$$

$$\tau = \tau_{\max}(1 - e^{-\frac{b}{k_0}}) \tag{6}$$

where:

σ_y - the positive pressure at depth y, [MPa]; n - the soil subsidence coefficient; k_1 - the soil cohesive deformation modulus coefficient; k_2 - the friction deforma

14 ption modulus coefficient; τ_{max} - the maximum shear stress at depth y, [MPa]; c_0 - soil cohesion N/mm^2; α - Soil internal friction angle; τ - the Simplified shear stress at depth y , [MPa]; k_0 - Shear deformation modulus coefficient.

When the digging shovel enters the soil, the positive pressure F_σ exerted by the soil on the digging shovel is:

$$F_\sigma = \frac{b}{\cos(\theta/2)}\int_0^b \sigma_y d_y \tag{7}$$

When the digging shovel enters the soil, the shear stress F_τ exerted by the soil on the digging shovel is:

$$F_\tau = \frac{b}{\cos(\theta/2)}\int_0^b \tau d_y \tag{8}$$

The penetration resistance F_{f2} is:

$$F_{f2} = 2F_\sigma \sin\frac{\alpha}{2} + 2F_\tau \cos\frac{\alpha}{2} \tag{9}$$

Positive pressure analysis and calculation

According to Rankine's earth pressure theory, a mechanical model of the digging shovel and the surrounding soil is established, as illustrated in Figure 3. In this model, the normal stress σ_z on the digging shovel at a depth of z is denoted, while q represents the normal pressure exerted by the soil on the digging shovel. Additionally, β indicates the angle of slip between the slip line and the plane of the shovel.

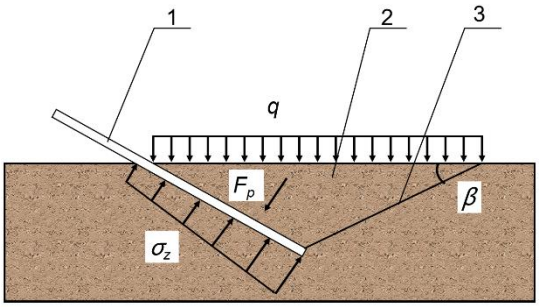

Fig. 3 - Stress analysis of shovel surface

1– Digging shovel; 2– Soil; 3– Slip line

σ_z is the normal stress and slip angle on the digging shovel at depth z:

$$\sigma_z = \gamma z \tan^2(\frac{\pi}{4} + \frac{\alpha}{2}) + q\tan^2(\frac{\pi}{4} + \frac{\alpha}{2}) + 2c_0 \tan^2(\frac{\pi}{4} + \frac{\alpha}{2}) \tag{10}$$

$$\beta = \frac{\pi}{4} - \frac{\alpha}{2} \tag{11}$$

According to Rankine earth pressure theory, the positive pressure of the soil on the digging shovel is:

$$F_p = b\int_0^b \sigma_z d_z \tag{12}$$

$$F_p = \frac{1}{2}\gamma b^3 \tan^2(\frac{\pi}{4} + \frac{\alpha}{2}) + qb^2 \tan^2(\frac{\pi}{4} + \frac{\alpha}{2}) + 2c_0 b^2 \tan^2(\frac{\pi}{4} + \frac{\alpha}{2}) \tag{13}$$

where: γ - the soil bulk density [N/mm^3].

Digging shovel resistance calculation

According to Figure 3, the soil slip volume V is:

$$V = \frac{b^2}{2\tan\beta} d \tag{14}$$

The inertial force of the soil on the digging shovel is:

$$F_a = \rho V a \tag{15}$$

where: ρ - the soil density [kg/mm^3]; a - the slip acceleration of soil relative to digging shovel [m/s^2].

The friction force of the soil on the digging shovel is:

$$F_{f1} = \mu F_p \tag{16}$$

where: μ - the kinetic friction factor between soil and digging shovel.

To sum up, the total resistance F of the sliding soil to the digging shovel is:

$$F = \sqrt{(F_{f1} + F_{f2})^2 + (F_p + F_a)^2} \tag{17}$$

According to the formula presented above, the width of the digging shovel, the depth to which it penetrates the soil, and the angle of the shovel tip all influence the digging resistance encountered during operation. In practical cassava harvesting, the conditions are complex and variable. The digging resistance is also affected by factors such as the size and shape of soil particles, soil moisture content, crop growth conditions, and other related variables.

Bionic cassava digging shovel design

Bionic prototype

The excavation device, as the primary component of the potato harvester, significantly influences both the operational efficiency of the machine and the quality of the harvested potato products. Within this excavation device, the excavation shovel teeth serve as the core elements that impact soil crushing and operational resistance. This article selects the adult Giron rabbit, a breed derived from California cave rabbits in the United States, as the bionic model. To maintain the stability of their burrows, Giron rabbits typically excavate in soil characterized by higher viscosity and hardness *(Liu et al., 2010)*. The bionic sample rabbit measures 44 cm in length, 20 cm in height, and has a front foot width of 3 cm, with its front toe claws illustrated in Figure 4.

a) original photo b) Black & white photo

Fig. 4 - Bionic prototype rabbit paw

Digging shovel design

To obtain a comprehensive three-dimensional point cloud map of the toe claws, a high-precision 3D object scanner (supplied by Beijing Tianyuan 3D Technology Co., Ltd., with a scanning accuracy of up to 0.023 mm and a resolution of up to 0.02 mm) was utilized to perform a 360-degree scan of the toe claws, thereby establishing a three-dimensional point cloud model. Subsequently, the three-dimensional point clouds were processed and denoised using FreeScan Trak software, resulting in a three-dimensional image in STL format, as illustrated in Figure 5.

Fig. 5 - 3D cloud point diagram of bionic prototype rabbit paw toe

The front toe of the rabbit paw serves as the primary tool for digging holes. The unique biological curvature of its outer contour is the key factor that ensures effective soil cutting performance *(Yu et al., 2019; Jia et al., 2019)*. The outline curve of the front toe is illustrated in Figure 6. To obtain a true and reliable representation of the outer contour curve of the toe claw, coordinate data from the cloud point diagram were extracted, and polynomial fitting was performed on this data using MATLAB. The resulting four distinct outer contour curves are presented in Figure 7. The fitting degree (R^2) of the contour curve equations exceeds 0.99, confirming that the accuracy of the extracted outer contour curve aligns with the actual biometric curve, thus meeting the necessary fitting requirements.

The equation is:

$$y_1 = 9.606\times10^{-11}x^4 - 1.767\times10^{-7}x^3 - 1.449\times10^{-4}x^2 + 0.3919x + 82.65 \quad (18)$$

$$y_2 = -2.329\times10^{-10}x^4 + 4.934\times10^{-7}x^3 - 6.256\times10^{-3}x^2 + 0.3979x + 328.1 \quad (19)$$

$$y_3 = 1.97\times10^{-15}x^6 - 6.836\times10^{-12}x^5 + 9.182\times10^{-9}x^4 - 5.881\times10^{-6}x^3 + 1.81\times10^{-3}x^2 - 0.138 \quad (20)$$

$$y_4 = -2.02\times10^{-15}x^6 + 6.373\times10^{-12}x^5 - 7.336\times10^{-9}x^4 + 3.6\times10^{-6}x^3 - 5.621\times10^{-4}x^2 + 0.04x + 345.7 \quad (21)$$

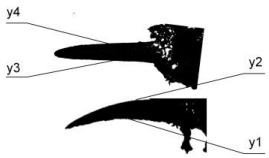

Fig. 6 - Bionic model rabbit paw outer contour

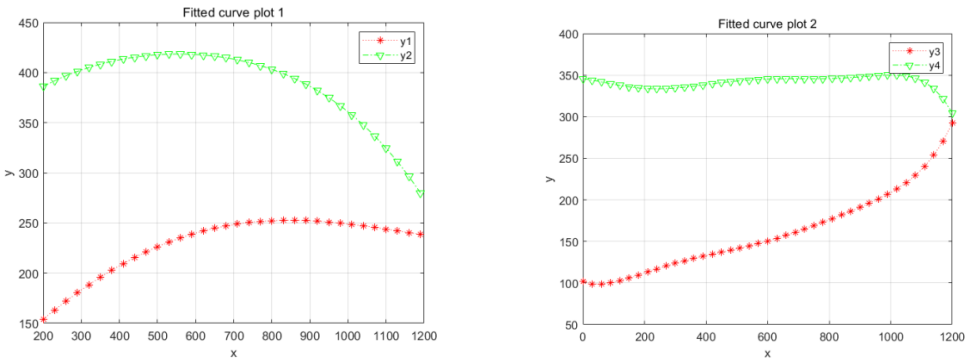

a) y_1 and y_2 curve b) y_3 and y_4 curve

Fig. 7 - Outer contour function curve graph

Using the aforementioned contour curve equation as a reference, the outer contour surface of the bionic shovel is reconstructed utilizing SolidWorks software *(Yu et al., 2022; Shi et al., 2014)*. The bionic shovel teeth are designed as fitting surfaces, with the side view projection curve serving as the horizontal reconstruction curve. Curve y_1 is designated as the upper ridge line, while curve y_2 represents the lower ridge line. The outer contour curves of the shovel blade are identified as curves y_3 and y_4. Consequently, a three-dimensional model of bionic shovel type 1 is established, as illustrated in Figure 8b. To this model, a bionic claw arch structure is incorporated, resulting in the creation of three-dimensional bionic shovel type 2, as depicted in Figure 8c. Additionally, a control group consisting of ordinary shovel teeth is included to establish a three-dimensional model of a conventional shovel, as shown in Figure 8a. For the bionic shovel, θ is the angle between the tangents of curves y_3 and y_4, and the intersection of the tangents is the same as that of the conventional shovel of the same specification.

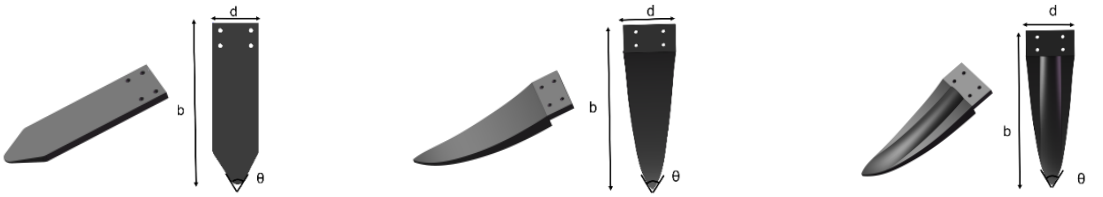

a) A conventional shovel; b) Bionic shovel type 1; c) Bionic shovel type 2;

Fig. 8 - Excavating shovel 3D model

b – Digging shovel length; c – Digging shovel width; θ – Digging blade angle

Discrete element simulation experiment

Discrete element model of soil and its cassava

Research indicates that an increase in the number of Discrete Element Method (DEM) particles can significantly enhance simulation efficiency while maintaining calculation accuracy, albeit with an increase in computation time *(Yang et al., 2018; Zhou et al., 2023)*. Consequently, this article categorizes soil particles into four distinct types. Additionally, a five-point sampling method was employed to collect soil samples from the experimental field. Following the screening of these samples through a soil sieve, it was noted that soil particles larger than 5 mm, as well as those ranging from 2 mm to 5 mm in diameter, exhibited irregular shapes. Specifically, particles exceeding 5 mm were confirmed to be irregularly shaped. For modelling purposes, particles larger than 5 mm were represented using a four-sphere model, while those measuring between 2 mm and 5 mm were represented with a three-sphere model. Particles smaller than 2 mm were found to be approximately spherical, leading to the selection of a single-sphere model for this category. The classification of particle types and sizes is illustrated in Figure 9.

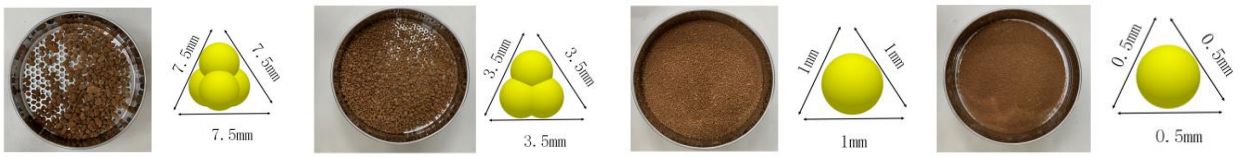

a) Soil particles above 5 mm; b) 2-5 mm soil particles; c) 1-2 mm soil particles; d) Soil particles below 1mm;

Fig. 9 - Soil particle discrete element model

During the cassava harvesting process, cassava stems are a primary focus of research regarding the fragmentation of the cassava-soil complex. This paper presents findings from a field investigation conducted at the Experimental Base of the Tropical High Efficiency Crops Agricultural Machinery Research Institute in Danzhou City, Hainan Province. The study revealed that cassava exhibits a growth pattern characterized by numerous tubers and straight, elongated stems. Most cassava stem models are approximately evenly distributed across the eight spatial quadrants *(Yang et al., 2022)*. Additionally, in the cassava planting area, physical parameters of the cassava were collected through direct measurements and averaged. The stem length can reach up to 60 cm, with a radius of about 4 m and an average depth of approximately 30 cm after maturity. The cassava stem itself measures around 30 cm. This article employs SolidWorks software to create a three-dimensional model, which is then saved and imported into EDEM for rapid particle filling. The discrete element model of cassava tubers is illustrated in Figure 10.

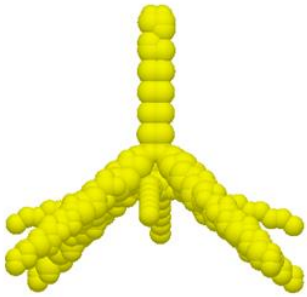

Fig. 10 - Cassava discrete element model

EDEM discrete element simulation model and its parameter settings

Hainan Province is situated in a tropical environment characterized by high temperatures and humidity. The accumulation of organic matter in this region facilitates the formation of red soil, which exhibits high viscosity resistance and significant thickness. Notably, the rainy soil in Hainan tends to adhere to cassava digging shovels. To simplify the calculation model, this article treats the soil as a viscous body. The "Hertz-Mindlin and JKR" contact model employs viscous particles as the theoretical foundation for analyzing the aggregation and separation motions between these particles *(Ding et al., 2017; Yang et al., 2015; Abo et al., 2004)*. Given the physical properties of Hainan's red soil, this paper adopts the "Hertz Mindlin with JKR Cohesion" contact model as the collision contact model for soil particles *(Sridhar et al., 2010; Mouazen et al., 2002)*. The physical parameters utilized in the simulation materials *(Wu et al., 2020)* are presented in Table 1.

Table 1

Material parameters and contact parameters

Parameter	Value
Density of soil particles / (kg·m^{-3})	1656
Density of shovel / (kg·m^{-3})	7850
Poisson's ratio of soil	0.45
Poisson's ratio of shovel	0.3
Shear modulus of soil / Pa	1.5×10^{6}
Shear modulus of shovel / Pa	7.1×10^{10}
Coefficient of static friction for soil-soil	0.41
Coefficient of rolling friction for soil-soil	0.35
Coefficient of restitution for soil-soil	0.43
Coefficient of static friction for soil–shovel	0.56
Coefficient of rolling friction for soil-shovel	0.18
Coefficient of restitution for soil-shovel	0.56
Cohesion interaction of soil-soil / (J·m^{-2})	7.90
Cohesion interaction of soil-shovel / (J·m^{-2})	6.10

Discrete element complex of cassava-soil

Based on an on-site agronomic investigation conducted at the Tropical High Efficiency Crop Agricultural Machinery Institute in Danzhou City, Hainan Province, the distribution patterns of soil particles were analyzed, the field shape was measured, and the cassava planting conditions were documented. The cassava-soil complex vector model is illustrated in Figure 11. The field ridges are designed to be trapezoidal, with specified lower and upper bottom widths. The plant spacing and ridge spacing are also defined. Measurements of soil compactness using instruments indicate that greater soil depth correlates with increased pressure. This article categorizes the terraced field ridges into three layers based on depth: deep soil, middle soil, and shallow soil. Following the stabilization of particles in EDEM, they are introduced into the excavation device of the cassava harvester. In Recurdyn, the motion pair of the excavation device is added, with the start mode set from 0 s to 1 s, allowing for a gradual acceleration to 300 mm/s via a linear function, after which it maintains a constant speed. In the post-processing interface, the resistance of the shovel teeth and the disturbance of soil particles during the operation of each type of shovel are analyzed.

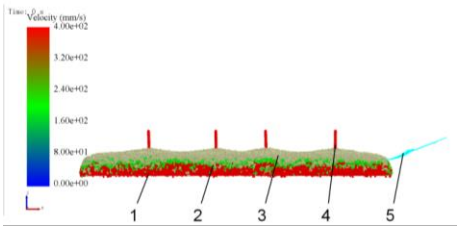

Fig. 11 - EDEM simulation diagram

1– Deep soil; 2– Middle soil; 3– Shallow soil; 4– Cassava; 5– Digging shovel

Simulation results and analysis

Comparative analysis of soil particle breaking ability

The impact of the excavating shovel on soil bonding is illustrated in Figure 12. Figure 12a demonstrates that after the soil bonding is disrupted by the blade of the ordinary excavating shovel, the bonding does not change once the soil reaches the shovel surface. Conversely, Figure 12b indicates that after the soil enters the shovel surface of bionic excavating shovel type 1, the bonding key increases along the curvature radius of the shovel surface, leading to an increase in force. As shown in Figure 12c, when the soil interacts with the shovel surface of bionic excavating shovel type 2, the arch structure significantly damages the bonding between soil particles. A portion of the soil slides upward along the shovel surface and enters the transition plate process, while some soil particles overcome the bonding force and slide laterally back to the ground.

Consequently, the primary working resistance of the excavating shovel arises from the reaction force of the soil against the transition plate. Therefore, reducing the amount of soil entering the transition plate can effectively decrease the working resistance.

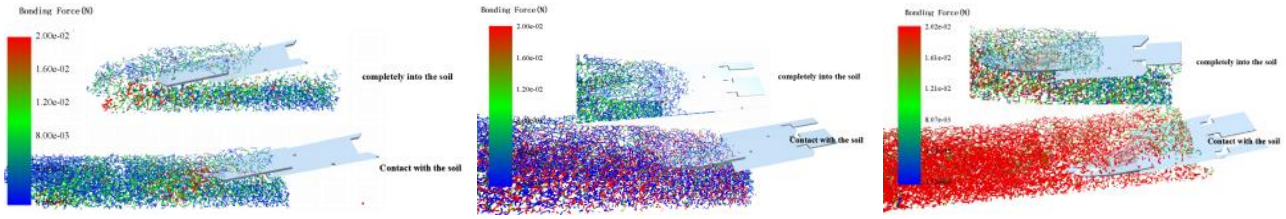

a) Ordinary digging shovel; b) Bionic shovel type 1; c) Bionic shovel type 2;

Fig. 12- Distribution diagram of soil particle cohesion force of digging shovel

Comparative analysis of excavation resistance

In the simulation, the forward speed of the frame is set to 300 mm/s, the soil penetration angle is set to 15°, the excavation depth is set to 40 mm, and the total simulation test time is set to 4 s. The simulation results are illustrated in the accompanying figure 13. Notably, the resistance experienced by the bionic digging shovel type 2 is significantly lower than that of the ordinary digging shovel and bionic digging shovel type 1. As depicted in Figure 13, the resistance of the excavating shovel increases sharply upon initial contact with the soil, reaching a stable value after 3 s. Consequently, this study considers the average value of the data from 3 s to 4 s as the resistance of the excavating shovel. The excavation depth achieved is 310 mm. At depths of 290 mm and 270 mm, the excavation resistance of the bionic excavating shovel type 1 is reduced by 6.84%, 4.58%, and 4.84% compared to the ordinary shovel, yielding an average reduction of 5.42%. In contrast, the excavation resistance of the bionic excavating shovel type 2 is reduced by 9.21%, 9.89%, and 10.12% relative to the ordinary shovel, with an average reduction of 9.74%. These results indicate a significant decrease in soil penetration resistance. The results show that bionic shovel type 2 is more effective.

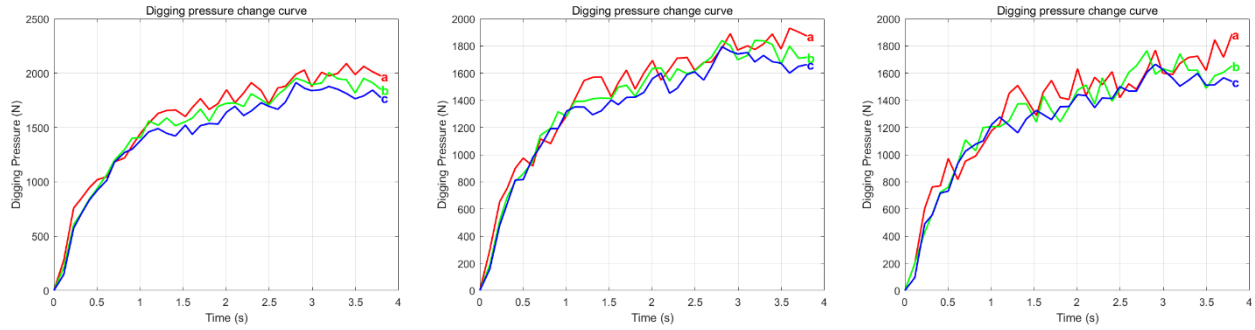

a) Excavation depth 310 mm; b) Excavation depth 290 mm; c) Excavation depth 270 mm;

Fig. 13- Resistance curves for 3 excavation depths

a– A conventional shovel; b– Bionic shovel type 1; c– Bionic shovel type 2

Optimization test of structural parameters of bionic shovel

Experimental factors

According to the resistance analysis, the width of the digging shovel, the depth of its penetration into the soil, and the angle of the shovel tip are the primary factors influencing the resistance generated during its operation *(Tagar et al., 2015; Barr et al., 2018)*. To identify the optimal combination of structural parameters for the bionic shovel type 2, simulations of excavations with various parameter combinations are conducted within a consistent simulation environment. These combinations are evaluated based on excavation resistance and soil breakage rate, where the soil breakage rate λ is defined as follows:

$$\lambda = \frac{N_0 - N_1}{N_0} \tag{22}$$

where:

λ - Soil damage rate;

N_1 - Bonding Number at the ending of simulation;

N_0 - Bonding Number at the start of simulation.

According to the agronomic inspection of the planting site, the spacing between cassava planting rows is set at 1 m to 1.2 m. To maintain an appropriate gap between the digging shovels while completely excavating the cassava stems, this article specifies the digging shovel width to be between 65 mm and 85 mm. Additionally, to analyze the depth of the cassava stems buried in the soil, the excavation blade width is established at 220 mm to 260 mm *(Xiong et al., 2022)*. To achieve a better drag reduction effect during excavation without compromising the excavation efficiency, the inclination angle of the excavation blade is recommended to be between 55° and 60° *(Fan et al., 2020)*. To simplify the number of experiments and minimize simulation errors, the Box-Behnken Design (BBD) experimental design was employed, resulting in 17 groups of orthogonal experiments encompassing 3 factors and 3 levels. The experimental factors of bionic shovel type 2 are coded as presented in table 2.

Table 2

Test factor coding table

Coded value	Factor		
	Digging shovel length *b*) A(mm)	Digging shovel width (*d*) B(mm)	Digging blade angle (*θ*) C(°)
-1	220	65	50
0	240	75	55
1	260	85	60

Test result analysis

After adjusting the physical dimensions of the excavating shovel in accordance with the 17 sets of test parameters, import the modified shovel design into the EDEM software. Conduct simulated excavation on the same soil model and record both the resistance encountered by the excavating shovel and the soil fragmentation rate during the excavation process. The results are presented in table 3.

Table 3

Simulation test results

Serial number	Digging shovel length A (mm)	Digging shovel width B (mm)	Digging blade angle C (°)	Digging Resistance（N）	Soil breakage rate *λ*
1	-1	-1	0	1733.66	91.4
2	1	-1	0	1939.54	92
3	-1	1	0	1972.14	92.7
4	1	1	0	2078.01	93.4
5	-1	0	-1	1851.07	92.4
6	1	0	-1	2034.9	92.7
7	-1	0	1	1928.46	93.6
8	1	0	1	2051.42	94
9	0	-1	-1	1823.09	91.7
10	0	1	-1	2055.59	92.6
11	0	-1	1	1830.46	93
12	0	1	1	2067.5	93.4
13	0	0	0	2007.4	92.3
14	0	0	0	2012.5	92.7
15	0	0	0	2013.72	92.4
16	0	0	0	2030.36	91.8
17	0	0	0	2033.2	92.6

Regression model establishment and significance testing

To conduct a comprehensive analysis of the effects of excavation blade length, width, and inclination angle on working resistance, variance analysis was performed on the test results, as presented in the tables 4 and 5.

According to the variance analysis results presented in the table 4, it can be concluded that the empirical significance value of the regression model is F = 55.15, P < 0.0001. The simulated linear terms, including shovel tooth length (A) and shovel tooth width (B), as well as the quadratic terms (A^2 and B^2), significantly impact excavation resistance, with extreme significance (P < 0.01). Furthermore, the quadratic term AB also has a significant effect on excavation resistance (P < 0.05). Consequently, the order of influence of each individual factor on excavation resistance is as follows: tooth width (B) > tooth length (A) > blade inclination angle (C). Other factors do not have a significant impact. After eliminating the insignificant terms, the coded regression equation for soil resistance is obtained:

$$Y_1 = 2019.436 + 77.3175A + 105.81125B - 25.0025AB - 33.148A^2 - 55.4505B^2 \quad (23)$$

According to the variance analysis results for the soil fragmentation rate presented in Table 5, the empirical significance value of the regression model is F = 6.82 and P = 0.0096. The simulated first-order factors, specifically the shovel tooth width (B) and blade inclination angle (C), have a highly significant impact on the soil fragmentation rate (P < 0.01). Additionally, the quadratic term C^2 demonstrates a significant effect on the soil fragmentation rate (P < 0.05). The table indicates that the order of influence of each individual factor on the soil fragmentation rate is as follows: blade inclination angle (C) > blade tooth width (B) > blade tooth length (A), while other factors do not exhibit a significant influence.

After removing the insignificant terms, the coded regression equation for the soil fragmentation rate is obtained:

$$Y_2 = 165.419375 + 0.52125B - 2.2105C + 0.0223C^2 \quad (24)$$

Table 4

Work resistance variance analysis

Source	Sum of Squares	*df*	Mean Square	*F*	*p*
Model	1.64×10^5	9	18162	55.15	< 0.0001
A(**)	47823.97	1	47823.97	145.22	< 0.0001
B(**)	89568.17	1	89568.17	271.97	< 0.0001
C	1601.5	1	1601.5	4.86	0.0632
AB(*)	2500.5	1	2500.5	7.59	0.0283
AC	926.29	1	926.29	2.81	0.1374
BC	5.15	1	5.15	0.0156	0.904
A^2(**)	4626.48	1	4626.48	14.05	0.0072
B^2(**)	12946.35	1	12946.35	39.31	0.0004
C^2	1654.95	1	1654.95	5.03	0.0599
Residual	2305.32	7	329.33		
Lack of Fit	1770.89	3	590.3	4.42	0.0926
Pure Error	534.43	4	133.61		
Cor Total	1.66×10^5	16			

Note: (**) indicates that the item is extremely significant (P<0.01), (*) indicates that the item is significant (P<0.05).

Table 5

Variance analysis of soil breakage rate

Source	Sum of Squares	*df*	Mean Square	*F*	*p*
Model	7.03	9	0.7815	6.82	0.0096
A	0.5	1	0.5	4.36	0.0751
B(**)	2	1	2	17.46	0.0041
C(**)	2.64	1	2.64	23.09	0.002
AB	0.0025	1	0.0025	0.0218	0.8867
AC	0.0025	1	0.0025	0.0218	0.8867

Source	Sum of Squares	*df*	Mean Square	*F*	*p*
BC	0.0625	1	0.0625	0.5455	0.4842
A^2	0.2792	1	0.2792	2.44	0.1625
B^2	0.2476	1	0.2476	2.16	0.185
C^2(*)	1.31	1	1.31	11.42	0.0118
Residual	0.802	7	0.1146		
Lack of Fit	0.31	3	0.1033	0.8401	0.5385
Pure Error	0.492	4	0.123		
Cor Total	7.84	16			

Note: (**) indicates that the item is extremely significant ($P < 0.01$), (*) indicates that the item is significant ($P < 0.05$).

Response surface analysis and target optimization

The response surface is illustrated in Figure 14. The interactive effect of blade length A and blade width B on excavation resistance is depicted in Figure 14a. With the blade inclination angle C fixed at 0 coded value and blade length A held constant, an increase in shovel width B leads to a rise in excavation resistance. This increase is pronounced in the range of 65-75 mm and more gradual in the range of 75-85 mm. Conversely, when shovel tooth width B is kept constant, excavation resistance increases with an increase in shovel tooth length A. The change is significant in the range of 220-240 mm, becomes more gradual in the range of 240-260 mm, and exhibits a slight downward trend after reaching a plateau. The interactive effect of blade length A and blade inclination angle C on excavation resistance is shown in Figure 14b. When blade tooth width B is fixed at 0 coded value and blade tooth length A remains unchanged, excavation resistance does not exhibit significant changes as blade inclination angle C increases, although there is a slight upward trend at higher excavation resistances. The interactive effect of shovel tooth width B and blade inclination angle C on excavation resistance is presented in Figure 14c. When shovel tooth length A is fixed at 0 coded value and shovel tooth width B remains constant, excavation resistance does not show significant changes with an increase in blade inclination angle C. However, when blade inclination angle C is held constant, excavation resistance tends to increase as shovel tooth width B increases.

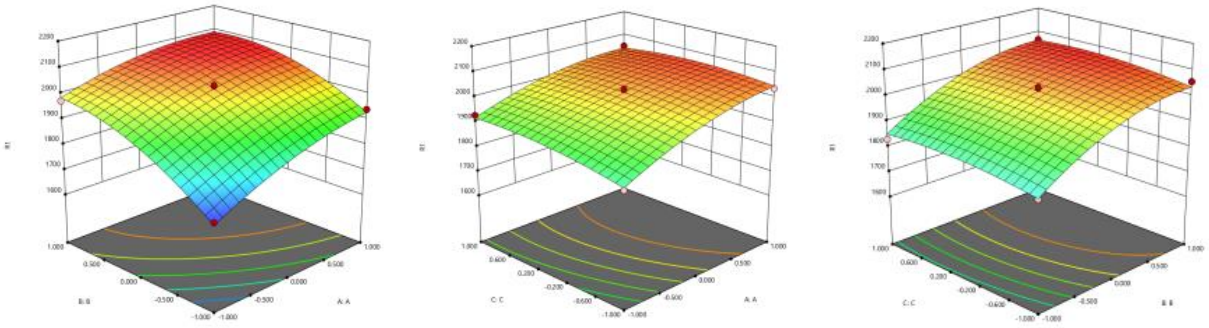

a) Response surface plots of A and B; b) Response surface plots of A and C; c) Response surface plots of B and C;

Fig. 14 - Excavation resistance response surface plot

The response surface is illustrated in Figure 15. The interactive effect of shovel tooth length A and shovel tooth width B on the soil breakage rate is depicted in Figure 15a. When the blade inclination angle C is fixed at 0 coded value and the shovel tooth length A remains constant, there is a slight upward trend in the soil crushing rate as the shovel width B increases, although this trend is not pronounced. Conversely, when the shovel tooth width B is held constant, the soil breakage rate does not exhibit significant changes with increasing shovel tooth length A. The interactive effect of shovel tooth length A and blade inclination angle C on the soil fragmentation rate is shown in Figure 15b.

When the shovel tooth width B is fixed at 0 coded value and the shovel tooth length A remains unchanged, the soil fragmentation initially decreases as the blade inclination angle C increases, then subsequently increases. Similarly, when the blade inclination angle C is held constant, soil fragmentation first decreases and then increases with an increase in blade length A. The interactive effect of blade width B and blade inclination angle C on the soil fragmentation rate is illustrated in Figure 15c. For a fixed shovel tooth length A at 0 coded value and constant shovel tooth width B, an increase in the blade inclination angle C results in a decrease in soil crushing, followed by an increase. When the blade inclination angle C remains constant, an increase in shovel tooth width B leads to a gradual increase in digging resistance.

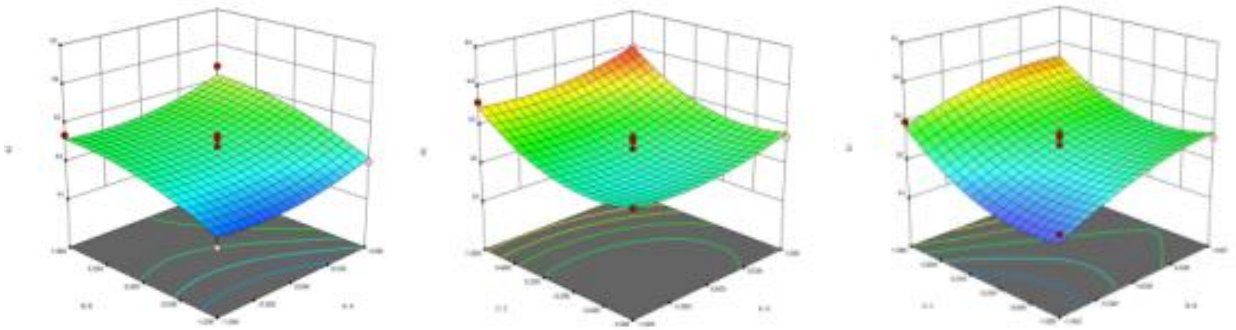

a) Response surface plots of A and B; b) Response surface plots of A and C; c) Response surface plots of B and C

Fig. 15 - Soil breakage rate response surface plot

In order to obtain the optimal bionic shovel parameters with smaller excavation resistance and larger soil breakage rate, this paper performs an optimal horizontal combination of test factors and establishes a mathematical model based on the boundaries of the test factors as follows:

$$s.t\begin{Bmatrix}\min Y_1\\ \max Y_2\\ 220mm \le x_1 \le 260mm\\ 65mm \le x_2 \le 85mm\\ 50^\circ \le x_3 \le 60^\circ\end{Bmatrix} \quad (25)$$

In the multi-objective optimization module of the Design Expert 13 software, the optimal parameter combination for the bionic shovel, which achieves both minimal excavation resistance and a higher soil breakage rate, consists of a shovel tooth length of 220 mm, a shovel tooth width of 65.1 mm, and a shovel edge inclination angle of 60°. This combination results in an excavation resistance of 1733.66 N and a maximum soil fragmentation rate of 92.9%. A simulation test was conducted using this optimal parameter combination in EDEM, yielding an excavation resistance of 1671.51 N and a soil fragmentation rate of 93.1%. The error between the predicted response value and the experimental value was within 5%, thereby verifying both the accuracy and reliability of the model.

RESULTS

Field test machines and materials

The test machine utilized in this study, as illustrated in the accompanying figure 16, primarily comprises a depth shape prevention device, an excavation device, a vibration separation device, a secondary transmission and sorting table, and a central control unit. The depth shape prevention device is designed to control and stabilize the working excavation depth. The shovel teeth of the excavation device crush the soil, which is subsequently directed into the vibration separation device via a connecting plate to facilitate the separation of potato soil. Finally, the material is conveyed to the secondary transmission and sorting platform for manual sorting. This secondary transmission effectively integrates mechanical separation of the potato soil, while manual sorting significantly mitigates damage to the cassava caused by collisions.

Fig. 16 - Soil breakage rate response surface plot

1– Power unit; 2– Control device; 3– Track; 4– Vibrating wheel; 5– Hydraulic device; 6– Excavation device; 7– Alignment device; 8– Frame; 9– Support wheel; 10– Separating screen; 11– Power supply unit; 12– Sorting table drive shaft; 13– Anti-collision device; 14– Secondary transmission sorting table

The excavation device of the cassava harvester is illustrated in the figure 17. It primarily consists of shovel teeth, connecting plates, and transition plates. The shovel teeth measure 220 mm in length and 65 mm in width, while the transition plate measures 980 mm in length and 300 mm in width. To facilitate testing, the connecting plate features openings. The fixed holes allow for the installation of two types of bionic shovel teeth, one type of ordinary shovel teeth, and transition plates onto the cassava harvester's excavation device. Additionally, a pressure sensor is installed at the bottom of the shovel to measure the excavation resistance encountered during operation.

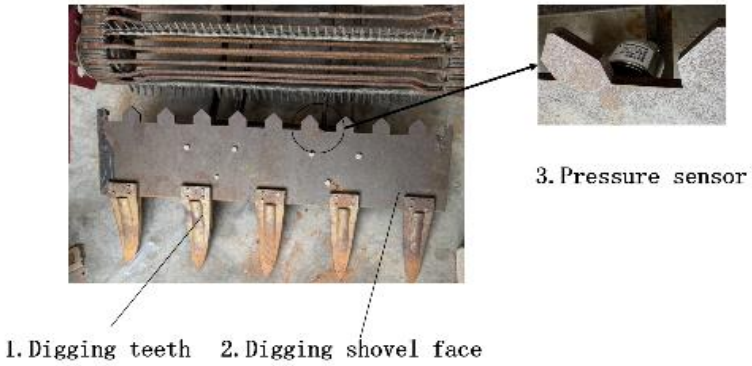

Fig. 17- Excavation device

1– Digging teeth; 2– Digging shovel face; 3– Pressure sensor

To verify the soil-breaking effect of bionic excavation, three types of digging shovels were installed on a cassava harvester for field tests conducted in the cassava planting base. The digging depth was set to 310 mm, and the forward speed was maintained at 300 mm/s. The results of the excavation effects on the ridge field are illustrated in Figure18. The image indicates that both the ordinary shovel and bionic shovel type 1 produced larger soil clumps. In contrast, bionic shovel type 2 resulted in a more uniform soil breakage, demonstrating superior performance, which aligns with the simulation results.

Fig. 18- Comparison chart of field excavation effects

1– Ordinary digging shovel; 2– Bionic shovel type 1; 3– Bionic shovel type 2

The spacing between the conveyor chains of the cassava harvester is 40 mm. Consequently, this paper employs a soil sieve with a diameter of 20 mm to conduct five sets of sampling screenings across three ridge fields. As shown in Table 6, the proportion of soil particles with a diameter of 20 mm or greater for ordinary shovels is 18.94%. In contrast, the bionic shovel type 1 has a soil particle diameter of 20 mm or greater accounting for 16.98%, while the bionic shovel type 2 shows that soil particles of 20 mm or greater comprise 11.92%. Thus, it can be concluded that the bionic shovel type 2 exhibits superior soil breaking ability compared to both the ordinary shovel and bionic shovel type 1.

Table 6

The proportion of surface soil diameter above 20

Sampling serial number	Bionic shovel type 1 (%)	Bionic shovel type 2 (%)	Ordinary digging shovel (%)
1	16.5	12.3	18.3
2	17.6	11.2	19.5
3	17.3	11.6	20.3
4	15.9	12.8	17.8
5	17.6	11.7	18.8
average value	16.98	11.92	18.94

Excavation resistance comparison test

The pressure sensor and information transmission module installed at the base of the digging shovel collect and transmit the excavation resistance values in real time. To simplify the testing process, the digging depth was set to 310 mm, and the forward speed was maintained at 300 mm/s. The resistance change curve over time is illustrated in Figure 19. Notably, the resistance value rapidly increases to a stable level upon entering the soil. It is evident that the resistance encountered by the bionic shovel type 2 is significantly lower than that experienced by the ordinary shovel and the bionic shovel type 1.

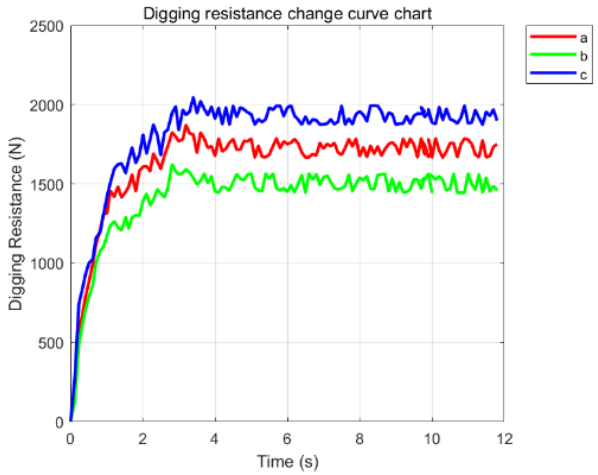

Fig. 19- Digging resistance change curve chart

a– Bionic shovel type 1; b– Bionic shovel type 2; c– Ordinary digging shovel

To ensure the accuracy of the data, each model of excavator shovel was tested 10 times, and the average data from 4 s to 12 s is shown in Figure 19. The results of the excavation resistance tests are presented in the table 7. The average resistance experienced by the Ordinary digging shovel during operation is 1886.842 N. The average resistance for Bionic shovel type 1 is 1729.390 N, and the average resistance for Bionic shovel type 2 is 1600.316 N. Calculations show that the resistance of the Type 1 Bionic Shovel is reduced by 8.34% compared to the conventional shovel. In addition, the Type 2 Bionic Shovel has a 15.19% reduction in resistance compared to a conventional digging shovel. In the simulation results in Figure 3, the digging depth is 310 mm, and the resistance of the Type 1 Bionic Shovel is reduced by 6.84% compared to the conventional shovel. Compared with the conventional shovel, the resistance of the Type 2 bionic shovel is reduced by 9.21%. The margin of error between simulation and experiment is within 10%, which verifies the reliability of the simulation. In terms of digging performance, the Type 2 Bionic Shovel outperforms the Normal Shovel and the Type 1 Bionic Shovel.

Table 7

The proportion of surface soil diameter above 20

Sampling serial number	Bionic shovel type 1 / (N)	Bionic shovel type 2 / (N)	Conventional digging shovel / (N)
1	1712.397	1627.799	1854.514
2	1721.62	1573.192	1872.327
3	1712.786	1617.638	1876.475
4	1710.114	1573.576	1871.152
5	1751.522	1569.991	1907.87
6	1714.208	1629.65	1903.715
7	1730.245	1570.074	1894.575
8	1753.198	1601.268	1906.316
9	1761.941	1629.691	1900.092
10	1725.87	1610.28	1881.385
average value	1729.39	1600.316	1886.842

CONCLUSIONS

This article presents the design of a cassava digging shovel specifically tailored for the extensive and dense red soils found in tropical regions. Utilizing a bionic rabbit claw toe biological curve structure, the shovel effectively reduces digging resistance and enhances the soil breakage rate during excavation tasks. The following conclusions are drawn:

1) Simulation test results for cassava digging indicate that at excavation depths of 310 mm, 290 mm, and 270 mm, the digging resistance of bionic digging shovel type 1 is reduced by 6.84%, 4.58%, and 4.84%, respectively, yielding an average reduction of 5.42% compared to the ordinary shovel. In contrast, the digging resistance of bionic digging shovel type 2 is decreased by 9.21%, 9.89%, and 10.12%, with an average reduction of 9.74%. The digging performance of bionic digging shovel type 2 significantly surpasses that of both bionic digging shovel type 1 and the ordinary shovel.

2) An analysis of the simulation test results reveals that the optimal parameter combination for bionic excavating shovel type 2 includes a tooth length of 220 mm, a tooth width of 65.1 mm, and a specific blade inclination, resulting in an excavation resistance of 1733.66 N and a substantial soil fragmentation rate of 92.9%.

3) Field test results demonstrate that bionic digging shovel type 2 possesses a superior ability to break soil, the Type 1 bionic digging shovel exhibits a reduction in resistance of 6.84%, while the Type 2 bionic digging shovel demonstrates a more significant reduction of 9.21%, in comparison to the traditional digging shovel achieving, thereby meeting the requirements for cassava harvesting.

ACKNOWLEDGEMENT

This work was funded by the National Natural Science Foundation of China, Research on the device and mechanism of low damage cassava coupled excavation based on dynamic rupture characteristics of cassava-soil complex, grant number 5226050106.

REFERENCES

[1] Abo E., Hamilton R., Boyle J. H., (2004), Simulation of soil blade interaction for sandy soil using advanced 3D finite element analysis, *Soil and Tillage Research*, vol. 75, pp. 61-73, Netherlands.

[2] Barr J. B., Ucgul D. J. M., Fielke J. M., (2018), Simulating the effect of rake angle on narrow opener performance with the discrete element method, *Biosystems Engineering*, vol. 171, ISSN 1537-5110, pp. 1-15, Netherlands.

[3] Cui G., Ma Y., Yang D., Jia J. X., Li Y., (2019), Research situation of bionic resistance reducing technology about potato digging shovel (马铃薯挖掘铲仿生减阻技术研究概况), *Agricultural Engineering*, vol. 9, ISSN 2095-1795, pp. 19-22, Beijing/China.

[4] Ding Q., Ren J., Belal E. A., Zhao J., Ge S., Li Y., (2017), Discrete element analysis of subsoiling process in wet sticky paddy soil (湿粘水稻土深松过程离散元分析), *Transactions of the Chinese Society for Agricultural Machinery*, vol. 48, ISSN 1000-1298, pp. 38-48, Beijing/China.

[5] Duanmu L., (2020), Design and research on bionic excavating shovel for cassava harvester (木薯收获机仿生挖掘铲减阻设计与研究), *Jilin University*, Jilin/China.

[6] Fan Y., (2020), Research on potato digging mechanism and bionic shovel design based on discrete element method (基于离散元法的马铃薯挖掘机理研究及仿生铲设计), *Shenyang Agricultural University*, Shenyang /China.

[7] Jia H., Guo M., Zhao J., Huang D., Zhuang J., (2019), Design and test of bionic wide-ridge soybean tilling-sowing machine, *International Journal of Agricultural and Biological Engineering*, vol. 12, ISSN 1934-6344, pp. 42-51, China.

[8] Li J., Li X., Hu B., Gu T., Wang Z., Wang H., (2023), Analysis of the resistance reduction mechanism of potato bionic digging shovels in clay and heavy soil conditions, *Computers and Electronics in Agriculture*, vol. 214, ISSN 1872-7107, pp. 1761-1761, Netherlands.

[9] Li X., Liu X., Mao Y., Chen X., (2014), Desalination effect of flue gas desulfurization gypsum on tidal flat soil in the Weishi area (烟气脱硫石膏对围室滩涂土壤的脱盐作用), *Journal of Environmental Engineering Technology*, vol. 6, ISSN 1674-991X, pp. 503-527, Beijing/China.

[10] Liu H., (2010), Understanding the living habits of rabbits (认识兔子的生活习性), *Jilin Animal Husbandry and Veterinary Medicine*, vol. 31, ISSN 1672-2078, pp. 40-40, Jilin/China.

[11] Mouazen A. M., Ramon H., (2002), A numerical–statistical hybrid modelling scheme for evaluation of draught requirements of a subsoiler cutting a sandy loam soil, as affected by moisture content, bulk

density and depth, *Soil and Tillage Research*, vol. 63, ISSN 0167-1987, pp. 155-165, Netherlands.
[12] Shi L., (2014), Design and simulation research on the potato bionic digging shovel, *Agricultural Research in the Arid Areas*, vol. 0, ISSN 1000-7601, pp. 0-0, China.
[13] Sridhar H., Richard W., Marklin, Paula E. P., Cariapa V., (2010), A Shovel With a Perforated Blade Reduces Energy Expenditure Required for Digging Wet Clay, *Human Factors*, vol. 52, ISSN 0018-7208, pp. 492-502, America.
[14] Sun J., Wang Y., Zhang S., Yun H., Jin T., Zhang Z., (2020), The mechanism of resistance-reducing / anti-adhesion and its application on biomimetic disc furrow opener, *Mathematical Biosciences and Engineering*, vol. 17, ISSN 1547-1063, pp. 4657-4677, Arizona State/America.
[15] Susila E., Hryciw R. D., (2003), Large displacement FEM modelling of the cone penetration test (CPT) in normally consolidated sand, *International Journal for Numerical and Analytical Methods in Geomechanics*, vol. 27, ISSN 0363-9061, pp. 585-602, United Kingdom.
[16] Tagar A. A., Ji C., Adamowski J., Malard J., Chen S., Ding Q., Abbasi N. A., (2015), Finite element simulation of soil failure patterns under soil bin and field testing conditions, *Soil and Tillage Research*, vol. 145, ISSN 0167-1987, pp. 157-170, Netherlands.
[17] Wu P., Zhang X., Li Y., Li M., Dong X., Liang D., (2020), Study on the accumulation characteristics of lateritic soil model based on discrete element method (基于离散元的砖红土壤模型堆积特性研究) , *Journal of Agricultural Mechanization Research*, vol. 42, ISSN 1003-188X, pp. 145-150, Heilongjiang /China.
[18] Xiong C., Zhou D., Deng G., Li G., Cui Z., He F., Li L., (2022), Design and testing of an automatic control system for digging depth of a vibrating chain cassava harvester (振动链式木薯收获机挖掘深度自动控制系统设计与测试) , *Journal of Huazhong Agricultural University (Natural Science Edition)*, vol. 41, ISSN 1000-2421, pp. 217-226, Hubei /China.
[19] Yang J., Yang W., Yang J., (2022), Measurement of cassava stem parameters and EDEM simulation parameter calibration (木薯种茎参数测量及 EDEM 仿真参数标定), *Journal of Agricultural Mechanization Research*, vol. 44, ISSN 1003-188X, pp. 197-202, Heilongjiang /China.
[20] Yang W., Li J., Yang J., Wei L., (2015), Numerical Simulation of An Experienced Farmer Lifting Tubers of Cassava for Designing A Bionic Harvester , *CMES-Computer Modeling in Engineering & Science*, vol. 104, ISSN 1526-1492, pp. 471-491, America.
[21] Yang Y., Tong J., Ma Y., Li M., Jiang X., Li J., (2018), Design and experiment of bionic soil-cutting blade based on the multi-toe structure characteristics of mole rats (基于鼹鼠多趾结构特征的仿生切土刀片设计与试验), *Transactions of the Chinese Society for Agricultural Machinery*, vol. 49, ISSN 1000-1298, pp. 122-128, Beijing/China.
[22] Yu J., Ma Y., Wang S., Xu Z., Liu X., Wang H., Qi H., Han L., Zhuang J., (2022), 3D Finite Element Simulation and Experimental Validation of a Mole Rat's Digit Inspired Biomimetic Potato Digging Shovel, *Applied sciences,* vol. 12, ISSN 2076-3417, pp. 108315-108315, Switzerland.
[23] Yu J., Wang R., Tong X., Zou W., (2019), Surface reconstruction of rabbit claws and extraction of characteristic curves (兔子爪趾曲面重构及特征曲线的提取), *Journal of Chinese Agricultural Mechanization*, vol. 40, ISSN 2095-5553, pp. 43-47, Jiangsu/China.
[24] Zhang C., Zhao Z., (2015), Advanced Kinematics (高等机构学), *China Machine Press*, Beijing/China.
[25] Zhang Z., Xue H., Wang Y., Xie K., Deng Y., (2022), Design and experiment of Panax notoginseng bionic excavating shovel based on EDEM (基于离散元法的三七仿生挖掘铲设计与试验), *Transactions of the Chinese Society for Agricultural Machinery*, vol. 53, ISSN 1000-1298, pp. 100-111, Beijing/China.
[26] Zhao C., Bai B., (2017), Principles of Soil Mechanics (土力学原理), *Tsinghua University Press*, Beijing/China.
[27] Zhao J., Lu Y., Guo M., Fu J., Wang Y., (2021), Design and experiment of bionic stubble breaking-deep loosening combined tillage machine, *International Journal of Agricultural and Biological Engineering*, vol. 14, ISSN 1934-6344, pp. 123-134, China.
[28] Zhou W., Xue N., Song K., Nuan W., Wang J., Fu Q., Na M., Tang H., Wang Q., (2023), Bionic Optimization Design and Discrete Element Experimental Design of Carrot Combine Harvester Ripping Shovel. *Processes*, vol. 11, ISSN 2227-9717, pp. 1526-1526, Switzerland.
[29] Zou X., Liao Y., Ma Q., Liu S., Zhu D., (2013), Bionic design and finite element analysis of excavating shovel for cassava harvester (木薯收获机挖掘铲仿生设计及其有限元分析), *Science Technology and Engineering*, vol. 13, ISSN 1671-1815, pp. 10122-10128, Beijing/China.